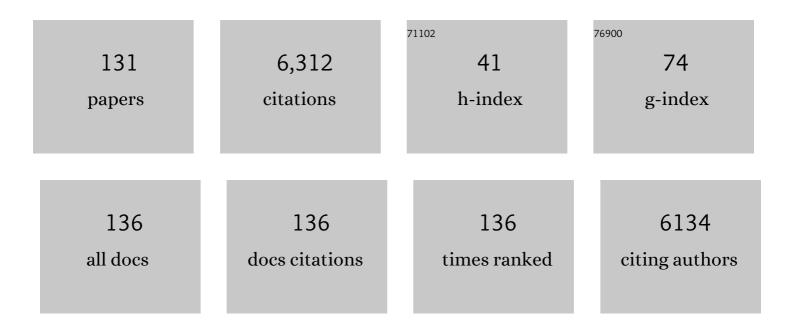
## Zheming Wang

List of Publications by Year in descending order

Source: https://exaly.com/author-pdf/3346763/publications.pdf Version: 2024-02-01



#	Article	IF	CITATIONS
1	c-Type Cytochrome-Dependent Formation of U(IV) Nanoparticles by Shewanella oneidensis. PLoS Biology, 2006, 4, e268.	5.6	310
2	Structure of a bacterial cell surface decaheme electron conduit. Proceedings of the National Academy of Sciences of the United States of America, 2011, 108, 9384-9389.	7.1	301
3	The roles of outer membrane cytochromes of <i>Shewanella</i> and <i>Geobacter</i> in extracellular electron transfer. Environmental Microbiology Reports, 2009, 1, 220-227.	2.4	285
4	lsolation of a High-Affinity Functional Protein Complex between OmcA and MtrC: Two Outer Membrane Decaheme c -Type Cytochromes of Shewanella oneidensis MR-1. Journal of Bacteriology, 2006, 188, 4705-4714.	2.2	227
5	Identification and Characterization of MtoA: A Decaheme c-Type Cytochrome of the Neutrophilic Fe(II)-Oxidizing Bacterium Sideroxydans lithotrophicus ES-1. Frontiers in Microbiology, 2012, 3, 37.	3.5	186
6	Rapid electron exchange between surface-exposed bacterial cytochromes and Fe(III) minerals. Proceedings of the National Academy of Sciences of the United States of America, 2013, 110, 6346-6351.	7.1	179
7	A transâ€outer membrane porinâ€cytochrome protein complex for extracellular electron transfer by <scp><i>C</i></scp> <i>eobacter sulfurreducens</i> â€ <scp>PCA</scp> . Environmental Microbiology Reports, 2014, 6, 776-785.	2.4	178
8	Cryogenic Laser Induced Fluorescence Characterization of U(VI) in Hanford Vadose Zone Pore Waters. Environmental Science & Technology, 2004, 38, 5591-5597.	10.0	164
9	Reoxidation of Bioreduced Uranium under Reducing Conditions. Environmental Science & Technology, 2005, 39, 6162-6169.	10.0	157
10	In Situ Infrared Spectroscopic Study of Forsterite Carbonation in Wet Supercritical CO <sub>2</sub> . Environmental Science & Technology, 2011, 45, 6204-6210.	10.0	153
11	Contribution of Extracellular Polymeric Substances from <i>Shewanella</i> sp. HRCR-1 Biofilms to U(VI) Immobilization. Environmental Science & amp; Technology, 2011, 45, 5483-5490.	10.0	149
12	Influence of Calcite and Dissolved Calcium on Uranium(VI) Sorption to a Hanford Subsurface Sediment. Environmental Science & Technology, 2005, 39, 7949-7955.	10.0	137
13	Fluorescence spectroscopy of U(VI)-silicates and U(VI)-contaminated Hanford sediment. Geochimica Et Cosmochimica Acta, 2005, 69, 1391-1403.	3.9	136
14	Scaleâ€dependent desorption of uranium from contaminated subsurface sediments. Water Resources Research, 2008, 44, .	4.2	123
15	Direct Involvement of Type II Secretion System in Extracellular Translocation of <i>Shewanella oneidensis</i> Outer Membrane Cytochromes MtrC and OmcA. Journal of Bacteriology, 2008, 190, 5512-5516.	2.2	113
16	Dissolution of uranyl microprecipitates in subsurface sediments at Hanford Site, USA. Geochimica Et Cosmochimica Acta, 2004, 68, 4519-4537.	3.9	110
17	Adsorption study of selenium ions from aqueous solutions using MgO nanosheets synthesized by ultrasonic method. Journal of Hazardous Materials, 2018, 341, 268-276.	12.4	101
18	Facet-Specific Photocatalytic Degradation of Organics by Heterogeneous Fenton Chemistry on Hematite Nanoparticles. Environmental Science & Technology, 2019, 53, 10197-10207.	10.0	101

#	Article	IF	CITATIONS
19	Redox Reactions of Reduced Flavin Mononucleotide (FMN), Riboflavin (RBF), and Anthraquinone-2,6-disulfonate (AQDS) with Ferrihydrite and Lepidocrocite. Environmental Science & Technology, 2012, 46, 11644-11652.	10.0	98
20	Shape-preserving amorphous-to-crystalline transformation of CaCO <sub>3</sub> revealed by in situ TEM. Proceedings of the National Academy of Sciences of the United States of America, 2020, 117, 3397-3404.	7.1	97
21	Communication: Spectroscopic phase and lineshapes in high-resolution broadband sum frequency vibrational spectroscopy: Resolving interfacial inhomogeneities of "identical―molecular groups. Journal of Chemical Physics, 2011, 135, 241102.	3.0	96
22	Kinetics of Reduction of Fe(III) Complexes by Outer Membrane Cytochromes MtrC and OmcA of <i>Shewanella oneidensis</i> MR-1. Applied and Environmental Microbiology, 2008, 74, 6746-6755.	3.1	89
23	Characterization of lignin derived from water-only and dilute acid flowthrough pretreatment of poplar wood at elevated temperatures. Biotechnology for Biofuels, 2015, 8, 203.	6.2	86
24	Size and Morphology Controlled Synthesis of Boehmite Nanoplates and Crystal Growth Mechanisms. Crystal Growth and Design, 2018, 18, 3596-3606.	3.0	82
25	Boehmite and Gibbsite Nanoplates for the Synthesis of Advanced Alumina Products. ACS Applied Nano Materials, 2018, 1, 7115-7128.	5.0	79
26	A thermodynamic model for predicting mineral reactivity in supercritical carbon dioxide: I. Phase behavior of carbon dioxide–water–chloride salt systems across the H2O-rich to the CO2-rich regions. Chemical Geology, 2012, 322-323, 151-171.	3.3	78
27	Effect of co-solutes on the products and solubility of uranium(VI) precipitated with phosphate. Chemical Geology, 2014, 364, 66-75.	3.3	75
28	Hydrogenase―and outer membrane <i>c</i> â€ŧype cytochromeâ€facilitated reduction of technetium(VII) by <i>Shewanella oneidensis</i> MRâ€1. Environmental Microbiology, 2008, 10, 125-136.	3.8	74
29	Cryogenic Laser Induced U(VI) Fluorescence Studies of a U(VI) Substituted Natural Calcite:Â Implications to U(VI) Speciation in Contaminated Hanford Sediments. Environmental Science & Technology, 2005, 39, 2651-2659.	10.0	73
30	Superior lithium adsorption and required magnetic separation behavior of iron-doped lithium ion-sieves. Chemical Engineering Journal, 2018, 332, 160-168.	12.7	69
31	Effect of phosphate on U(VI) sorption to montmorillonite: Ternary complexation and precipitation barriers. Geochimica Et Cosmochimica Acta, 2016, 175, 86-99.	3.9	68
32	In Situ Infrared Spectroscopic Study of Brucite Carbonation in Dry to Water-Saturated Supercritical Carbon Dioxide. Journal of Physical Chemistry A, 2012, 116, 4768-4777.	2.5	61
33	Effect of Grain Size on Uranium(VI) Surface Complexation Kinetics and Adsorption Additivity. Environmental Science & Technology, 2011, 45, 6025-6031.	10.0	60
34	Adsorption of Uranyl on Gibbsite:  A Time-Resolved Laser-Induced Fluorescence Spectroscopy Study. Environmental Science & Technology, 2006, 40, 1244-1249.	10.0	56
35	Effect of Reaction Pathway on the Extent and Mechanism of Uranium(VI) Immobilization with Calcium and Phosphate. Environmental Science & amp; Technology, 2016, 50, 3128-3136.	10.0	52
36	A cryogenic fluorescence spectroscopic study of uranyl carbonate, phosphate and oxyhydroxide minerals. Radiochimica Acta, 2008, 96, 591-598.	1.2	51

#	Article	IF	CITATIONS
37	Carbon Paste Electrode Modified with Carbamoylphosphonic Acid Functionalized Mesoporous Silica: A New Mercury-Free Sensor for Uranium Detection. Electroanalysis, 2004, 16, 870-873.	2.9	46
38	Self-Exchange Electron Transfer Kinetics and Reduction Potentials for Anthraquinone Disulfonate. Journal of Physical Chemistry A, 2004, 108, 3292-3303.	2.5	46
39	Continuous, One-pot Synthesis and Post-Synthetic Modification of NanoMOFs Using Droplet Nanoreactors. Scientific Reports, 2016, 6, 36657.	3.3	45
40	Fe <sub>3–<i>x</i></sub> Ti <sub><i>x</i></sub> O <sub>4</sub> Nanoparticles as Tunable Probes of Microbial Metal Oxidation. Journal of the American Chemical Society, 2013, 135, 8896-8907.	13.7	43
41	Comparative reactivity study of forsterite and antigorite in wet supercritical CO2 by in situ infrared spectroscopy. International Journal of Greenhouse Gas Control, 2013, 18, 246-255.	4.6	43
42	Transport of U(VI) through sediments amended with phosphate to induce in situ uranium immobilization. Water Research, 2015, 69, 307-317.	11.3	43
43	Sustainable Disposal of Cr(VI): Adsorption–Reduction Strategy for Treating Textile Wastewaters with Amino-Functionalized Boehmite Hazardous Solid Wastes. ACS Sustainable Chemistry and Engineering, 2018, 6, 6811-6819.	6.7	43
44	Uranium Phases in Contaminated Sediments below Hanford's U Tank Farm. Environmental Science & Technology, 2009, 43, 4280-4286.	10.0	42
45	Cr(III) Adsorption by Cluster Formation on Boehmite Nanoplates in Highly Alkaline Solution. Environmental Science & Technology, 2019, 53, 11043-11055.	10.0	42
46	Reductive dissolution of goethite and hematite by reduced flavins. Geochimica Et Cosmochimica Acta, 2013, 121, 139-154.	3.9	41
47	Effects of soluble flavin on heterogeneous electron transfer between surface-exposed bacterial cytochromes and iron oxides. Geochimica Et Cosmochimica Acta, 2015, 163, 299-310.	3.9	41
48	The Effect of pH and Time on the Extractability and Speciation of Uranium(VI) Sorbed to SiO <sub>2</sub> . Environmental Science & Comp; Technology, 2012, 46, 6604-6611.	10.0	38
49	Particle size effect and the mechanism of hematite reduction by the outer membrane cytochrome OmcA of Shewanella oneidensis MR-1. Geochimica Et Cosmochimica Acta, 2016, 193, 160-175.	3.9	38
50	Luminescence spectroscopic study of europium(III) and terbium(III) with ethylenediamine in dimethyl sulfoxide. Journal of the Chemical Society Dalton Transactions, 1993, , 2791.	1.1	37
51	Phosphate-Induced Immobilization of Uranium in Hanford Sediments. Environmental Science & Technology, 2016, 50, 13486-13494.	10.0	37
52	Characterization of uranium-contaminated sediments from beneath a nuclear waste storage tank from Hanford, Washington: Implications for contaminant transport and fate. Geochimica Et Cosmochimica Acta, 2010, 74, 1363-1380.	3.9	36
53	Determining individual mineral contributions to U(VI) adsorption in a contaminated aquifer sediment: A fluorescence spectroscopy study. Geochimica Et Cosmochimica Acta, 2011, 75, 2965-2979.	3.9	35
54	Near-infrared spectroscopic investigation of water in supercritical CO2 and the effect of CaCl2. Fluid Phase Equilibria, 2013, 338, 155-163.	2.5	34

#	Article	IF	CITATIONS
55	Identification and Characterization of UndA <sub>HRCR-6</sub> , an Outer Membrane Endecaheme <i>c</i> -Type Cytochrome of Shewanella sp. Strain HRCR-6. Applied and Environmental Microbiology, 2011, 77, 5521-5523.	3.1	32
56	Synthesis of 2D Hexagonal Hematite Nanosheets and the Crystal Growth Mechanism. Inorganic Chemistry, 2019, 58, 16727-16735.	4.0	32
57	Dehydration of the Uranyl Peroxide Studtite, [UO <sub>2</sub> (Î- <sup>2</sup> -O <sub>2</sub> )(H <sub>2</sub> O) <sub>2</sub> ]Â-2H <sub>2</sub> O, Affords a Drastic Change in the Electronic Structure: A Combined X-ray Spectroscopic and Theoretical Analysis, Inorganic Chemistry, 2018, 57, 1735-1743.	4.0	31
58	The dissolution of synthetic Na-boltwoodite in sodium carbonate solutions. Geochimica Et Cosmochimica Acta, 2006, 70, 4836-4849.	3.9	30
59	Inhibition Effect of Secondary Phosphate Mineral Precipitation on Uranium Release from Contaminated Sediments. Environmental Science & Technology, 2009, 43, 8344-8349.	10.0	30
60	Transport and retention of engineered nanoporous particles in porous media: Effects of concentration and flow dynamics. Colloids and Surfaces A: Physicochemical and Engineering Aspects, 2013, 417, 89-98.	4.7	30
61	Spectroscopic study of ion binding in synthetic polyelectrolytes using lanthanide ions. Inorganica Chimica Acta, 1995, 239, 139-143.	2.4	27
62	Europium Uptake and Partitioning in Oat (Avena sativa) Roots as Studied by Laser-Induced Fluorescence Spectroscopy and Confocal Microscopy Profiling Technique. Environmental Science & Technology, 2003, 37, 5247-5253.	10.0	27
63	<i>In Situ</i> Synthesis of γ-AlOOH and Synchronous Adsorption Separation of V(V) from Highly Concentrated Cr(VI) Multiplex Complex solutions. ACS Sustainable Chemistry and Engineering, 2017, 5, 6674-6681.	6.7	27
64	Kinetics of Microbial Reduction of Solid Phase U(VI). Environmental Science & Technology, 2006, 40, 6290-6296.	10.0	25
65	In-Situ Measurements of Engineered Nanoporous Particle Transport in Saturated Porous Media. Environmental Science & Technology, 2010, 44, 8190-8195.	10.0	25
66	Microbial Reduction of Intragrain U(VI) in Contaminated Sediment. Environmental Science & Technology, 2009, 43, 4928-4933.	10.0	24
67	The solubility product of NaUO2PO4·xH2O determined in phosphate and carbonate solutions. Radiochimica Acta, 2005, 93, 401-408.	1.2	23
68	Atomic Origins of the Self-Healing Function in Cement–Polymer Composites. ACS Applied Materials & Interfaces, 2018, 10, 3011-3019.	8.0	23
69	Direct Observation of the Orientational Anisotropy of Buried Hydroxyl Groups inside Muscovite Mica. Journal of the American Chemical Society, 2019, 141, 2135-2142.	13.7	23
70	Luminescence from thetrans-Dioxotechnetium(V) Chromophore. Journal of the American Chemical Society, 2005, 127, 14978-14979.	13.7	22
71	Influence of calcium on microbial reduction of solid phase uranium(VI). Biotechnology and Bioengineering, 2007, 97, 1415-1422.	3.3	22
72	Incorporation of Np(V) and U(VI) in carbonate and sulfate minerals crystallized from aqueous solution. Geochimica Et Cosmochimica Acta, 2015, 151, 133-149.	3.9	21

#	Article	IF	CITATIONS
73	Photo-production of reactive oxygen species and degradation of dissolved organic matter by hematite nanoplates functionalized by adsorbed oxalate. Environmental Science: Nano, 2020, 7, 2278-2292.	4.3	21
74	Surface Hydration and Hydroxyl Configurations of Gibbsite and Boehmite Nanoplates. Journal of Physical Chemistry C, 2020, 124, 5275-5285.	3.1	21
75	A fluorescence spectroscopic study on the speciation of Cm(III) and Eu(III) in the presence of organic chelates in highly basic solutions. Radiochimica Acta, 2003, 91, 329-338.	1.2	20
76	Biotic and Abiotic Reduction and Solubilization of Pu(IV)O2•xH2O(am) as Affected by Anthraquinone-2,6-disulfonate (AQDS) and Ethylenediaminetetraacetate (EDTA). Environmental Science & Technology, 2012, 46, 2132-2140.	10.0	20
77	Excited States and Luminescent Properties of UO <sub>2</sub> F <sub>2</sub> and Its Solvated Complexes in Aqueous Solution. Inorganic Chemistry, 2014, 53, 7340-7350.	4.0	20
78	The energetic basis for hydroxyapatite mineralization by amelogenin variants provides insights into the origin of <i>amelogenesis imperfecta</i> . Proceedings of the National Academy of Sciences of the United States of America, 2019, 116, 13867-13872.	7.1	20
79	Electronic and Molecular Structures oftrans-Dioxotechnetium(V) Polypyridyl Complexes in the Solid State. Inorganic Chemistry, 2011, 50, 5815-5823.	4.0	19
80	Transformation of Gibbsite to Boehmite in Caustic Aqueous Solution at Hydrothermal Conditions. Crystal Growth and Design, 2019, 19, 5557-5567.	3.0	19
81	The role of surface hydroxyls on the radiolysis of gibbsite and boehmite nanoplatelets. Journal of Hazardous Materials, 2020, 398, 122853.	12.4	18
82	Crystallographic and Spectroscopic Characterization of Americium Complexes Containing the Bis[(phosphino)methyl]pyridine-1-oxide (NOPOPO) Ligand Platform. Inorganic Chemistry, 2018, 57, 2278-2287.	4.0	17
83	Investigation of U(VI) Adsorption in Quartz–Chlorite Mineral Mixtures. Environmental Science & Technology, 2014, 48, 7766-7773.	10.0	16
84	Electrochemistry and Spectroelectrochemistry of Luminescent Europium Complexes. Electroanalysis, 2016, 28, 2109-2117.	2.9	16
85	Fluorescence anisotropy studies of molecularly imprinted polymers. Luminescence, 2006, 21, 7-14.	2.9	15
86	The aqueous complexation of thorium with citrate under neutral to basic conditions. Radiochimica Acta, 2006, 94, .	1.2	15
87	Photophysics and Luminescence Spectroelectrochemistry of [Tc(dmpe) <sub>3</sub> ] <sup>+/2+</sup> (dmpe = 1,2- <i>bis</i> (dimethylphosphino)ethane). Journal of Physical Chemistry A, 2013, 117, 12749-12758.	2.5	15
88	Scintillation and luminescence in transparent colorless single and polycrystalline bulk ceramic ZnS. Journal of Luminescence, 2015, 157, 416-423.	3.1	15
89	Can Cr( <scp>iii</scp> ) substitute for Al( <scp>iii</scp> ) in the structure of boehmite?. RSC Advances, 2016, 6, 107628-107637.	3.6	15
90	Uranium Release from Acidic Weathered Hanford Sediments: Single-Pass Flow-Through and Column Experiments. Environmental Science & Technology, 2017, 51, 11011-11019.	10.0	15

#	Article	IF	CITATIONS
91	Vibrational studies of saccharide-induced lipid film reorganization at aqueous/air interfaces. Chemical Physics, 2018, 512, 104-110.	1.9	15
92	Crystallization and Phase Transformations of Aluminum (Oxy)hydroxide Polymorphs in Caustic Aqueous Solution. Inorganic Chemistry, 2021, 60, 9820-9832.	4.0	15
93	Trends in Ln(III) Sorption to Quartz Assessed by Molecular Dynamics Simulations and Laser-Induced Fluorescence Studies. Journal of Physical Chemistry C, 2011, 115, 21120-21127.	3.1	14
94	Long-term kinetics of uranyl desorption from sediments under advective conditions. Water Resources Research, 2014, 50, 855-870.	4.2	14
95	Organic Enrichment at Aqueous Interfaces: Cooperative Adsorption of Glucuronic Acid to DPPC Monolayers Studied with Vibrational Sum Frequency Generation. Journal of Physical Chemistry A, 2019, 123, 5621-5632.	2.5	14
96	Thermodynamic model for the solubility of ThO2(am) in the aqueous Na+-H+-OH–NO3–H2O-EDTA system. Radiochimica Acta, 2003, 91, .	1.2	13
97	Complexation of Cm(III)/Eu(III) with silicates in basic solutions. Radiochimica Acta, 2005, 93, 741-748.	1.2	11
98	Fluorescent Functionalized Mesoporous Silica for Radioactive Material Extraction. Separation Science and Technology, 2012, 47, 1507-1513.	2.5	11
99	Insights into sorption speciation of uranium on phlogopite: Evidence from TRLFS and DFT calculation. Journal of Hazardous Materials, 2022, 427, 128164.	12.4	11
100	Time-Resolved Fluorescence Anisotropies in Mixed Surfactant Solutions. Journal of Colloid and Interface Science, 1999, 218, 260-264.	9.4	10
101	Atmospheric $\hat{l}^2$ -Caryophyllene-Derived Ozonolysis Products at Interfaces. ACS Earth and Space Chemistry, 2019, 3, 158-169.	2.7	10
102	Two-step route to size and shape controlled gibbsite nanoplates and the crystal growth mechanism. CrystEngComm, 2020, 22, 2555-2565.	2.6	10
103	Uranium fate in Hanford sediment altered by simulated acid waste solutions. Applied Geochemistry, 2015, 63, 1-9.	3.0	9
104	Spatially Resolved U(VI) Partitioning and Speciation: Implications for Plume Scale Behavior of Contaminant U in the Hanford Vadose Zone. Environmental Science & Technology, 2009, 43, 2247-2253.	10.0	8
105	Surface-Active β-Caryophyllene Oxidation Products at the Air/Aqueous Interface. ACS Earth and Space Chemistry, 2019, 3, 1740-1748.	2.7	8
106	Synthesis and surface spectroscopy of $\hat{l}\pm$ -pinene isotopologues and their corresponding secondary organic material. Chemical Science, 2019, 10, 8390-8398.	7.4	8
107	Radiation-Induced Interfacial Hydroxyl Transformation on Boehmite and Gibbsite Basal Surfaces. Journal of Physical Chemistry C, 2020, 124, 22185-22191.	3.1	8
108	Effect of Cr(III) Adsorption on the Dissolution of Boehmite Nanoparticles in Caustic Solution. Environmental Science & Technology, 2020, 54, 6375-6384.	10.0	8

#	Article	IF	CITATIONS
109	No Hydrogen Bonding between Water and Hydrophilic Single Crystal MgO Surfaces?. Journal of Physical Chemistry C, 2021, 125, 26132-26138.	3.1	8
110	Hydrogen bubbles and formation of nanoporous silicon during electrochemical etching. Surface and Interface Analysis, 2005, 37, 555-561.	1.8	7
111	Cooperative Adsorption of Trehalose to DPPC Monolayers at the Water–Air Interface Studied with Vibrational Sum Frequency Generation. Journal of Physical Chemistry B, 2019, 123, 8931-8938.	2.6	7
112	Studies on derivative fluorimetry. Part I. Determination of trace amounts of samarium, europium and terbium. Analyst, The, 1987, 112, 1081.	3.5	6
113	Observation of aqueous Cm(III)/Eu(III) and UO22+ nanoparticulates at concentrations approaching solubility limit by laser-induced fluorescence spectroscopy. Journal of Alloys and Compounds, 2006, 418, 166-170.	5.5	6
114	PowerSlicing to determine fluorescence lifetimes of water-soluble organic matter derived from soils, plant biomass, and animal manures. Analytical and Bioanalytical Chemistry, 2008, 390, 2189-2194.	3.7	6
115	Effect of Saline Waste Solution Infiltration Rates on Uranium Retention and Spatial Distribution in Hanford Sediments. Environmental Science & amp; Technology, 2008, 42, 1973-1978.	10.0	6
116	A spectroscopic study of the effect of ligand complexation on the reduction of uranium(VI) by anthraquinone-2,6-disulfonate (AH <sub>2</sub> DS). Radiochimica Acta, 2008, 96, 599-605.	1.2	6
117	The surface structure of α-uranophane and its interaction with Eu(III) – An integrated computational and fluorescence spectroscopy study. Geochimica Et Cosmochimica Acta, 2013, 103, 184-196.	3.9	6
118	Molecular Examination of Ion-Pair Competition in Alkaline Aluminate Solutions Using In Situ Liquid SIMS. Analytical Chemistry, 2021, 93, 1068-1075.	6.5	6
119	Quantitative determination of praesodymium(III)–neodymium(III)–holmium(III)–erbium(III) four-component systems by matrix–fourth derivative spectrophotometry. Analyst, The, 1994, 119, 2463-2466.	3.5	5
120	Artificial Aging of Phenanthrene in Porous Silicas Using Supercritical Carbon Dioxide. Environmental Science & Technology, 2001, 35, 3707-3712.	10.0	5
121	A Fluorescence-Based Method for Rapid and Direct Determination of Polybrominated Diphenyl Ethers in Water. Journal of Analytical Methods in Chemistry, 2015, 2015, 1-10.	1.6	5
122	Interdisciplinary Round-Robin Test on Molecular Spectroscopy of the U(VI) Acetate System. ACS Omega, 2019, 4, 8167-8177.	3.5	5
123	Simulation of solute transport through heterogeneous networks: analysis using the method of moments and the statistics of local transport characteristics. Scientific Reports, 2018, 8, 3780.	3.3	4
124	Experimental study of drying effects during supercritical CO2 displacement in a pore network. Microfluidics and Nanofluidics, 2018, 22, 1.	2.2	4
125	Americium incorporation into studtite: a theoretical and experimental study. Dalton Transactions, 2019, 48, 13057-13063.	3.3	4
126	Study on the Impacts of Capillary Number and Initial Water Saturation on the Residual Gas Distribution by NMR. Energies, 2019, 12, 2714.	3.1	4

#	Article	IF	CITATIONS
127	Evolution of Radicals from the Photolysis of High Ionic Strength Alkaline Nitrite Solutions. Journal of Physical Chemistry A, 2020, 124, 3019-3025.	2.5	4
128	Spectroscopic Elucidation of Lanthanide Cation Dissolution Mechanism in Borosilicate Glass. Materials Research Society Symposia Proceedings, 2001, 702, 1.	0.1	3
129	Use of Solvatochromism to Assay Preferential Solvation of a Prototypic Catalytic Site. Topics in Catalysis, 2015, 58, 258-270.	2.8	2
130	Identification of Fragile Microscopic Structures during Mineral Transformations in Wet Supercritical CO2. Microscopy and Microanalysis, 2013, 19, 268-275.	0.4	1
131	Steady-State Fluorescence Anisotropy Studies of Molecularly Imprinted Polymer Sensors. Materials Research Society Symposia Proceedings, 2003, 787, 331.	0.1	0